Available online at www.sciencedirect.com

SciVerse ScienceDirect

Geochimica et Cosmochimica Acta 93 (2012) 14–29

Geochimica et Cosmochimica Acta

www.elsevier.com/locate/gca

# The flux of iron and iron isotopes from San Pedro Basin sediments

Seth G. John [a,b,*], Jeffery Mendez [c,d], James Moffett [c], Jess Adkins [a]

[a] California Institute of Technology, Division of Geological and Planetary Sciences, Pasadena, CA 91125, USA
[b] University of South Carolina, Department of Earth and Ocean Sciences, Columbia, SC 29208, USA
[c] University of Southern California, Department of Biological Sciences, Los Angeles, CA 90033, USA
[d] California Institute of Technology, Division of Chemistry and Chemical Engineering, Pasadena, CA 91125, USA

Received 20 May 2011; accepted in revised form 3 June 2012; available online 23 June 2012

**Abstract**

Iron is an important nutrient in the ocean, but the different sources and sinks of iron are not well constrained. Here, we use measurements of Fe concentration and Fe stable isotope ratios to evaluate the importance of reducing continental margins as a source of Fe to the open ocean. Dissolved iron concentration ([Fe]) and iron stable isotope ratios ($\delta^{56}$Fe) were measured in the San Pedro and Santa Barbara basins. Dissolved $\delta^{56}$Fe ranges from −1.82‰ to 0.00‰ in the San Pedro Basin and from −3.45‰ to −0.29‰ in the Santa Barbara Basin, and in both basins the lowest $\delta^{56}$Fe values and highest Fe concentrations are found at the bottom of the basin reflecting the input of isotopically light Fe from reducing sediment porewaters. In the San Pedro Basin, we are also able to fingerprint an advective source of Fe from shallow continental shelves next to the basin and the atmospheric deposition of Fe into surface waters. A one-dimensional model of the Fe isotope cycle has been constructed for the deep silled San Pedro Basin. By fitting model output to data, values of several important iron cycle parameters are predicted including a flux of Fe from sediment porewaters into the water column of 0.32–1.14 μmol $m^{-2}$ $d^{-1}$, a first-order dissolved Fe precipitation rate constant of 0.0018–0.0053 $d^{-1}$, a flux $\delta^{56}$Fe of −2.4‰, and an isotope effect for Fe precipitation of $\Delta\delta^{56}Fe_{particulate\text{-}dissolved} = -0.8‰$. Applying our model-predicted Fe cycle parameters to the global ocean suggests that continental margins contribute 4–12% of world ocean dissolved Fe and make the ocean's Fe lighter by −0.08‰ to −0.26‰. The dramatically negative $\delta^{56}$Fe signature seen in the water column of the San Pedro and Santa Barbara basins demonstrate the utility of Fe isotopes as a tracer for continental margin Fe input from reducing sediments to the oceans, while the isotopic fractionation observed during loss of Fe from the dissolved phase suggests that this signature will be modified by subsequent reactions. Our modeling provides an initial framework for testing how these signals are transmitted into the open ocean.


## 1. INTRODUCTION

Iron is an important nutrient for phytoplankton growth in the oceans, but the sources of iron to the open ocean are poorly constrained. Atmospheric dust deposition has long been assumed to be an important source of iron to the surface ocean (e.g. Fung et al., 2000), but other sources such as hydrothermal vents and the release of Fe(II) from reducing continental-margin sediments might also be important sources of Fe to the open ocean (Johnson et al., 1999; Elrod et al., 2004; Bennett et al., 2008; Toner et al., 2009). Concentration measurements alone are often not sufficient to distinguish the provenance of marine iron, however Fe isotopes may provide a new tool for fingerprinting different sources of iron to the oceans.

High concentrations of dissolved Fe(II) are produced in reducing continental margin sediments, where insoluble Fe(III) can serve as the terminal electron acceptor in the degradation of organic material. This iron may eventually serve as a nutrient for phytoplankton growing in the surface

* Corresponding author at: University of South Carolina, Department of Earth and Ocean Sciences, Columbia, SC 29208, USA.
*E-mail address:* sjohn@geol.sc.edu (S.G. John).

0016-7037/$ - see front matter © 2012 Elsevier Ltd. All rights reserved.
http://dx.doi.org/10.1016/j.gca.2012.06.003

ocean, depending on how much Fe escapes from these sediments and is transported to surface waters in a dissolved and bioavailable form. Reducing continental margin sediments may therefore play an important role in the global marine Fe cycle, though they make up just a small fraction of the total ocean bottom surface area. Continental shelf iron is thought to play a particularly important role in coastal regions where upwelling provides a ready supply of other major nutrients (N, P, and Si) to surface waters (Johnson et al., 1999; Bruland et al., 2001, 2005; Lohan and Bruland, 2008). However, other studies have suggested that reducing continental margin sediments are an important source of Fe to the oceans even hundreds of kilometers from shore. Analysis of Fe-rich particles sampled in the central North Pacific suggests that they originated as Fe(II) diffusing from continental shelf sediments, and this Fe is hypothesized to support phytoplankton productivity far from shore in the HNLC North Pacific (Lam et al., 2006; Lam and Bishop, 2008). Global biogeochemical models have taken disparate approaches to parameterizing the importance of continental margin to the global Fe cycle. Some early models discounted continental margin sources, assuming that dust is the primary source of Fe to the oceans away from the coastline (e.g. Archer and Johnson, 2000; Parekh et al., 2004). Other models have found sediments to be an important source of Fe to the ocean, with the particular importance of reducing continental margin sediments accounted for either by prescribing a uniform sedimentary Fe flux above 1100 m (Moore et al., 2004), relating Fe flux to reduced carbon inputs (Moore and Braucher, 2008) or relating Fe flux to the extent of sedimentary anoxia (Aumont and Bopp, 2006). Efforts to directly quantify the flux of Fe from reducing sediments have used both porewater dissolved Fe concentration gradients (Sawlan and Murray, 1983; Elrod et al., 2004), and measurement of Fe concentrations in benthic flux chambers (Elrod et al., 2004; Severmann et al., 2010). Additionally, Fe fluxes have been predicted from organic carbon oxidation rates based on a global relationship established from benthic flux chamber data (Elrod et al., 2004). However, there can be large discrepancies between these various methods and between different deployments of the same method, as evidenced by the ~4 orders of magnitude spread in predictions of Fe flux in the San Pedro Basin from these previous studies, adding uncertainty to calculations of the global flux of Fe from reducing sediments.

Fe released from reducing sediments has a characteristically light $\delta^{56}Fe$ signature ($\delta^{56}Fe = (({}^{56}Fe/{}^{54}Fe)_{sample}/({}^{56}Fe/{}^{54}Fe)_{IRMM\text{-}014})$) which may help to trace and quantify the flux of Fe from continental margin sediments. The isotopically negative $\delta^{56}Fe$ signature of this sedimentary Fe reflects the fact that it originates as Fe(II), which is about 3‰ lighter than Fe(III) when the two species are at isotopic equilibrium (Johnson et al., 2002; Welch et al., 2003; Anbar et al., 2005). For example, porewater $\delta^{56}Fe$ values were −1.8‰ to −3.6‰ at the sediment–water interface at several locations along the Oregon-California continental shelf (Severmann et al., 2006, 2010) and −1.3‰ in bulk sediments on the Amazon shelf (Bergquist and Boyle, 2006). $\delta^{56}Fe$ measured in benthic flux chambers at eleven sites along the coast of California were generally between −0.7‰ and −4.0‰ (Severmann et al., 2010). However, it is not known how these $\delta^{56}Fe$ signatures are reflected in the overlying water column. Firstly, the large variability in Fe flux estimates may point to massive Fe precipitation near the sediment–water interface which could drastically alter the dissolved Fe isotope signature of the net Fe flux. Secondly, it is possible that the flux of reduced Fe from continental margins is complemented by a flux of dissolved Fe from oxic particle dissolution. For example, the isotopically positive ($\delta^{56}Fe = +0.37‰$) flux of Fe from the continental margin near New Guinea is inferred to be the result of oxic dissolution of sediments in the water column (Radic et al., 2011), and sediment porewaters from oxic deep-sea sediments in the Southern Ocean are isotopically similar to bulk crustal material ($\delta^{56}Fe = +0.12‰$) (Homoky et al., 2009). In order to distinguish between oxic and reductive fluxes of Fe from continental margins, and to determine the $\delta^{56}Fe$ of these fluxes, it is important to understand how [Fe] and $\delta^{56}Fe$ are modified in the water column after being released from sediments.

The borderland basins off the coast of California provide an ideal setting to examine the hypothesis that reducing continental margin sediments are an important source of iron to the open ocean. Coastal upwelling carries a large nutrient flux to surface waters which, in turn, fuels high productivity in surface waters and oxygen depletion below. While the areal extent of the California borderland basins is small, the intense biological productivity here impacts the entire North Pacific. The oxygen minimum zone intersecting with the borderland basins extends across the Pacific ocean, and the nitrate deficit ($N^*$) which is caused by denitrification in the California borderland basins affects nutrient availability over the whole North Pacific (Gruber and Sarmiento, 1997; Deutsch et al., 2001). The same low-oxygen conditions which lead to denitrification are responsible for the production of soluble Fe(II) in sediments, suggesting an important role in the global iron cycle if Fe produced at continental margins is transported into the open ocean. The San Pedro and Santa Barbara Basins are of particular interest because they have previously been well studied in terms of both physical and chemical oceanographic properties (Berelson, 1985, 1991; Berelson et al., 1982; Hammond et al., 1990). These silled basins are enclosed on all sides at the bottom, isolating them from cross currents and horizontal advection. Below the deepest sill, the distribution of properties in these basins can be described entirely in terms of one-dimensional vertical transport and reaction. Here, we employ recent analytical advances to measure the concentration and $\delta^{56}Fe$ of iron in the San Pedro and Santa Barbara Basins, and combine these measurements with simple models of iron transport and reaction in the deep basin to calculate key parameters such as the magnitude of Fe flux from the sediments, the timescale for Fe precipitation, the $\delta^{56}Fe$ of the flux, and the isotope effect for precipitation. These values provide a framework for predicting the impact of continental-margin derived iron on Fe concentrations and $\delta^{56}Fe$ in the world ocean.

## 2. METHODS

### 2.1. Oceanographic setting

#### 2.1.1. San Pedro Basin

The San Pedro Basin is located south of Los Angeles, California, USA (Fig. 1). The basin is approximately 10 by 20 km across, with broad shallow shelves between 0 and 100 m depth next to the basin, and a broad flat bottom at ~900 m. The basin is silled below 740 m. Because of high biological productivity in surface waters, oxygen concentrations in the deep waters are depleted. In the deepest San Pedro Basin, oxygen concentration can be as high as 10 μM after flushing events, but is more typically in the range of 2–5 μM (Berelson, 1991). The sediments are fully anoxic with dissolved iron concentrations as high as 100 μM (Severmann et al., 2010). We sampled the basin in September and October 2008 in conjunction with the San Pedro Ocean Timeseries (SPOT) cruises aboard the R/V Sea Watch. The basin is occasionally 'flushed' by a large input of cold, oxygen rich water into the basin (Berelson, 1991), but temperature data indicate that the time we sampled was a period of relative stagnation where the only input is a steady-state upwelling component that balances the influx of cold water into the bottom of the basin. Temperature profiles at the time of our sampling are similar to profiles taken during previous times when the basin had not been recently flushed (Berelson, 1991) (Fig. 2). Iron concentrations at depths of 750 and 800 m, where samples were taken in both September and October 2008, were the same within analytical error and $\delta^{56}$Fe measurements at these depths were very similar (Table 1). This suggests that the Fe cycle in the deep San Pedro Basin was at or near steady state during our sampling, making it possible to construct simple but realistic models of the iron isotope cycle using previous estimates of the rates of mixing and upwelling in the basin.

Estimates of the vertical turbulent diffusivity ($\kappa$) in the San Pedro Basin have been calculated using a wide variety of techniques. Hammond et al. compared the flux of $^{228}$Ra from sediments with the water column distribution of $^{228}$Ra to infer $\kappa$ between 1 and 3 cm$^2$ s$^{-1}$ (Hammond et al., 1990). Vertical profiles of nutrient concentrations, oxygen concentrations, temperature and salinity have been combined to calculate $\kappa$ at the 790 m horizon in the San Pedro Basin as $1.3 \pm 0.4$ cm$^2$ s$^{-1}$ (Berelson, 1991). Based on $^{222}$Rn concentrations in the San Pedro Basin, a value for $\kappa$ of $2.7 \pm 1.5$ cm$^2$ s$^{-1}$ was calculated (Berelson et al., 1982; Berelson and Hammond, 1986). The relationship between vertical diffusivity and density gradients can be used to calculate $\kappa$ of 1.1–2.4 cm$^2$ s$^{-1}$ for the San Pedro Basin between 750 and 900 m (Jackson, 1982). Overall, we use a range of $\kappa$ from 1 to 3 cm$^2$ s$^{-1}$.

#### 2.1.2. Santa Barbara Basin

The Santa Barbara Basin is located southwest of Santa Barbara, California. It is approximately 50 km long, 30 km across, 592 m deep, and is silled below 475 m. We sampled the basin on May 26, 2009 in conjunction with the second US Geotraces Intercalibration cruise aboard the R/V Knorr. Oxygen concentrations in the deepest Santa Barbara Basin can vary between 0 and 16 μM. Our nitrate concentration of 23 μM at 575 m is consistent with recent flushing of the basin (Reimers et al., 1990). Because of this recent flushing, and because our sampling resolution was much lower in the Santa Barbara Basin, we did not attempt a quantitative model of iron and iron isotope cycling in this basin.

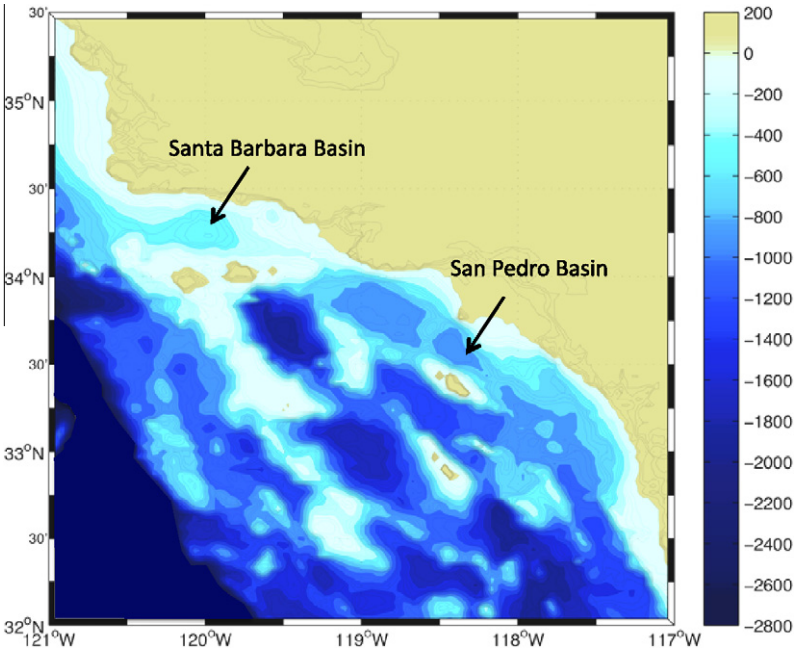


Fig. 1. Location of the San Pedro Basin and Santa Barbara Basin off the coast of southern California.

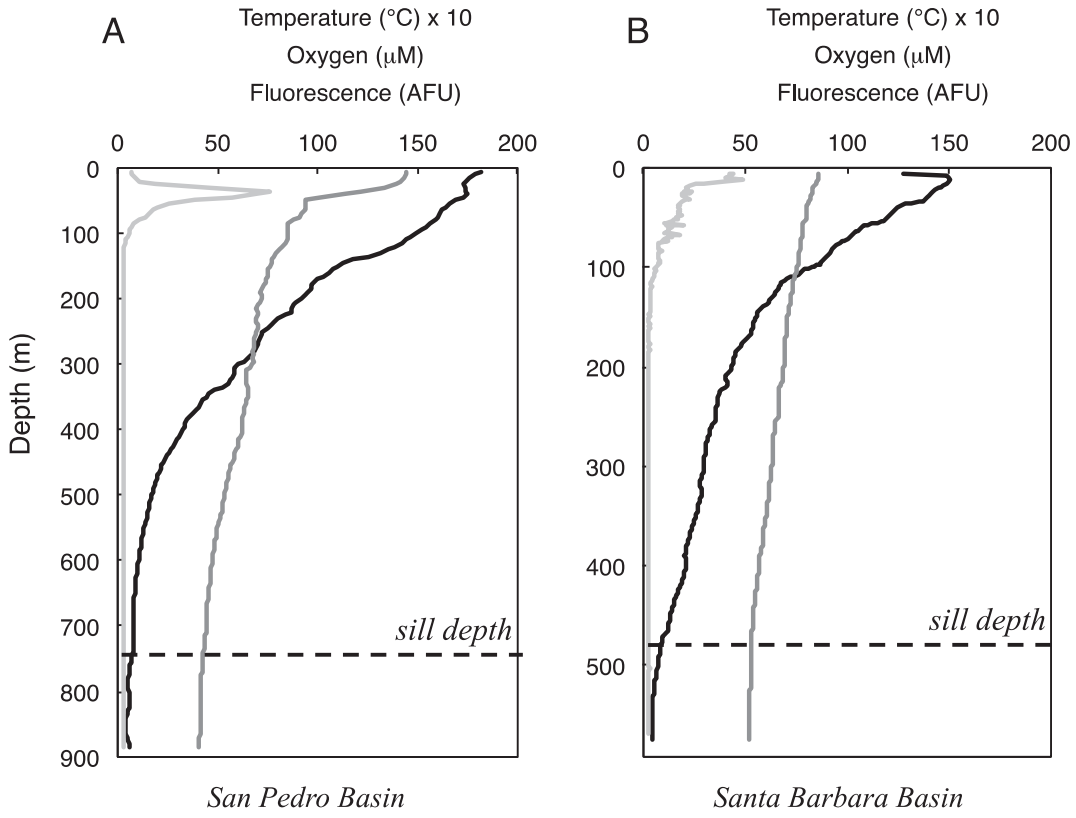


Fig. 2. Oceanographic parameters in the San Pedro basin (A) and Santa Barbara basin (B) at the time of sampling including temperature (dark gray line), oxygen concentration (black line), and fluorescence (light gray line).

### 2.2. Sample collection and storage

San Pedro Basin samples were mostly collected using 5 L Teflon-coated Niskin bottles mounted on a powder-coated rosette. The sample from 895 m was collected by mounting a single Teflon-coated Niskin on the outside of the ship's CTD rosette. The bottle was mounted at the very bottom of the rosette and was tripped while the CTD was moving downwards, so that the bottle was sampling clean water which was not contaminated by the rosette or hydrowire. Four liter water samples were filtered through 0.4 μm polyethersulfone filters (Pall Corporation) by overpressure with a small motorized pump on board the ship. Samples were acidified to pH 2 with HCl for storage within twelve hours of collection (Johnson et al., 2007).

Samples from the Santa Barbara Basin were collected using the US Geotraces trace-metal clean rosette equipped with Teflon-coated Niskin bottles, and filtered through an Osmonics Teflon filter capsule with a nominal pore size of 0.45 μm. One liter samples were acidified to pH 2 with HCl after 4 weeks at ambient pH, and allowed to sit for at least another 8 weeks at pH 2 in order to redissolve any precipitated Fe.

### 2.3. Seawater dissolved [Fe] and $\delta^{56}$Fe

Fe was extracted and purified for isotopic analysis according to previously developed methods for measurement of dissolved $\delta^{56}$Fe in seawater (John and Adkins, 2010). Briefly, Fe was extracted from pH 2 seawater onto an NTA-resin in a batch extraction process. Fe was eluted from the NTA resin in 10% HCl and further purified by anion exchange chromatography. Triplicate analyses of Fe stable isotope ratios were made on a Neptune multi-collector ICP-MS in high-resolution mode. $\delta^{56/54}$Fe and $\delta^{57/54}$Fe measurements were compared to ensure the absence of isobaric interferences. All $\delta^{56}$Fe ($\delta^{56/54}$Fe) measurements are reported against IRMM-014. External analytical errors for this method are typically 0.04‰ for seawater Fe concentrations as high as those in the San Pedro and Santa Barbara basins (John and Adkins, 2010) (Table 1).

San Pedro Basin seawater iron concentrations were measured by isotope dilution. While typical measurements of Fe concentration employ a high-resolution ICPMS instrument capable of optically separating the Fe beam from argide interferences (e.g. Wu and Boyle, 1998) or a multi-collector with a collision cell (e.g. Boyle et al., 2005), our method was optimized for analysis on an Agilent 7500 single-collector ICP-MS with a collision cell which aids in destruction of polyatomic interferences. 1.8 mL samples were spiked with $^{57}$Fe, and the iron was concentrated by co-precipitation with magnesium hydroxide (Wu and Boyle, 1998). The collision cell was used with 3 mL min$^{-1}$ $H_2$ and 2 mL min$^{-1}$ He. Signal intensities were measured at masses 44 (Ca), 56 (Fe) and 57 (Fe). A calcium standard was run in between samples to correct for $CaO^+$ and $CaOH^+$ interferences at masses 56 and 57. For samples with 1 nM Fe, typical blanks were 10% and <1% of the total sig-

Table 1
Iron concentration and stable isotope ratio data. Iron concentrations for all San Pedro Basin samples and the SAFe sample were measured by the same isotope dilution ICPMS method. Fe concentrations for the Santa Barbara Basin samples were calculated based on sample recovery assuming 89% extraction efficiency. Errors in $\delta^{56}$Fe are calculated according to John and Adkins (2010).

| Sampling date and location | Depth | Dissolved [Fe] (nM) | 2σ SE ($n = 3$) | Dissolved | |
|---|---|---|---|---|---|
| | | | | $\delta^{56}$Fe | 2σ SE |
| September, 2008 | 15 | 0.57 | 0.13 | 0.00 | 0.06 |
| San Pedro Basin | 15 | | | 0.01 | 0.06 |
| | 35 | 0.26 | 0.05 | −1.06 | 0.11 |
| | 35 | | | −0.87 | 0.11 |
| | 50 | 4.00 | 0.03 | −1.19 | 0.04 |
| | 50 | | | −1.23 | 0.04 |
| | 100 | 3.61 | 0.15 | −1.08 | 0.04 |
| | 100 | | | −1.11 | 0.04 |
| | 150 | 3.54 | 0.13 | −0.69 | 0.04 |
| | 150 | | | −0.73 | 0.04 |
| | 250 | 2.43 | 0.05 | −0.78 | 0.04 |
| | 250 | | | −0.85 | 0.04 |
| | 500 | 2.38 | 0.01 | −0.95 | 0.04 |
| | 500 | | | −0.99 | 0.04 |
| | 750 | 4.16 | 0.03 | −1.13 | 0.04 |
| | 750 | | | −1.21 | 0.04 |
| | 800 | 5.01 | 0.02 | −1.53 | 0.04 |
| | 800 | | | −1.57 | 0.04 |
| | 835 | 5.53 | 0.12 | −1.70 | 0.04 |
| | 835 | | | −1.76 | 0.04 |
| October, 2008 | 601 | 3.46 | 0.02 | −1.22 | 0.04 |
| San Pedro Basin | 651 | 3.36 | 0.07 | −1.31 | 0.04 |
| | 676 | 3.27 | 0.25 | −1.28 | 0.04 |
| | 700 | 3.21 | 0.14 | −1.21 | 0.04 |
| | 726 | 3.51 | 0.07 | −1.31 | 0.04 |
| | 751 | 4.08 | 0.08 | −1.44 | 0.04 |
| | 776 | 4.30 | 0.11 | −1.45 | 0.04 |
| | 801 | 4.85 | 0.07 | −1.55 | 0.04 |
| | 895 | 7.33 | 0.02 | −1.82 | 0.04 |
| May, 2010 | 10 | 1.6 | | −1.00 | 0.04 |
| Santa Barbara Basir | 30 | 2.7 | | −1.42 | 0.04 |
| | 60 | 3.2 | | −1.26 | 0.04 |
| | 110 | 4.3 | | −1.30 | 0.04 |
| | 160 | 4.2 | | −1.13 | 0.04 |
| | 230 | 5.4 | | −0.99 | 0.04 |
| | 330 | 5.9 | | −0.83 | 0.04 |
| | 380 | 6.6 | | −1.00 | 0.04 |
| | 430 | 8.8 | | −0.29 | 0.04 |
| | 480 | 9.7 | | −0.37 | 0.04 |
| | 530 | 12.3 | | −1.70 | 0.04 |
| | 560 | 29.5 | | −3.45 | 0.04 |
| SAFe D2 | | 0.95 | 0.12 | | |

nal intensity at masses 56 and 57, respectively. Typical Ca interferences were 3% and 18% of the total signal intensity at masses 56 and 57. Analytical precision was generally better than 0.15 nM (2σ SE). Our measurements of iron concentration in the SAFe D2 intercalibration standard using this method ($0.89 \pm 0.03$ nM, 2σ SE $n = 3$) matches well with the current consensus value ($0.923 \pm 0.029$ nM).

Fe concentrations in the Santa Barbara Basin were calculated based on the recovery of Fe onto the NTA resin and are estimated to be accurate within ~10%, based on using the same method in the San Pedro Basin comparing recoveries to concentration measured by isotope dilution ICPMS.

## 3. RESULTS

### 3.1. San Pedro Basin

Dissolved iron concentrations were measured for San Pedro Basin samples collected in September and October 2008 (Table 1, Fig. 3). At two depths in the silled basin where samples were collected at both times, iron concentrations were equal within analytical error and $\delta^{56}$Fe was very similar. In the full water column profile obtained by combing data from September and October 2008, three maxima in iron concentration are observed. The highest iron con-

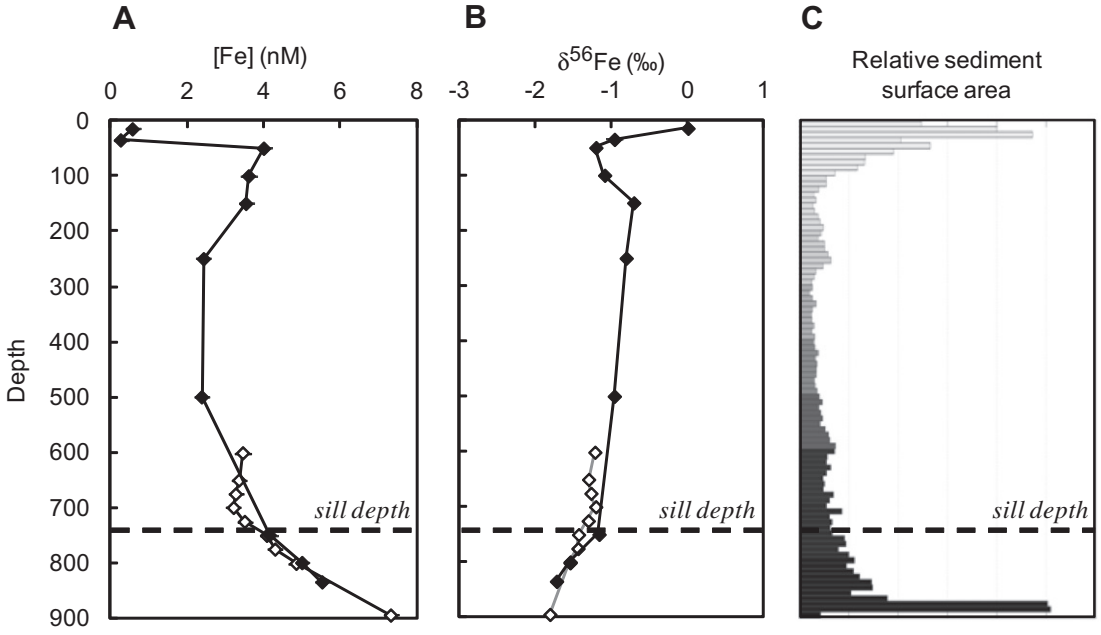


Fig. 3. Dissolved iron concentration (A) and $\delta^{56}$Fe (B) in the San Pedro Basin from samples collected in September 2008 (closed symbols) and October 2008 (open symbols). To a first approximation regions of high shelf area in the San Pedro Basin, as depicted in a histogram of basin topography (C), correspond to regions of high dissolved Fe concentrations and low $\delta^{56}$Fe.

centration of 7.33 nM was found at 895 m, just 5 m above the bottom of the basin. Moving up the water column, iron concentrations decrease towards mid-depths to a minimum at 500 m of [Fe] = 2.38 nM. From here iron concentrations slowly increase to a second maximum at 50 m, which is just below the mixed layer as defined by temperature gradients and the fluorescence maximum (Fig. 2). At 35 m, in the bottom of the mixed layer, we measure the lowest iron concentration in the whole profile of [Fe] = 0.26 nM. Closer to the surface, at 15 m, the iron concentration increases again for a third maximum of [Fe] = 0.57 nM. In the high-resolution sampling from October 2008, we observe a slight increase iron concentrations from [Fe] = 3.21 nM at 700 m to [Fe] = 3.46 nM at 600 m, which would suggest a fourth small maximum if data from September and October were considered as part of the same profile.

Dissolved $\delta^{56}$Fe values in the San Pedro Basin are, to a first approximation, the mirror image of Fe concentrations. The most dramatic [Fe] maxima, at 895 m near the bottom of the basin and at 50 m, are accompanied by minima in iron isotope ratios of $\delta^{56}$Fe = −1.82‰ and $\delta^{56}$Fe = −1.21‰, respectively. However, the maximum iron concentration in the surfacemost 15 m sample is accompanied not by an isotopically light $\delta^{56}$Fe signature, but by the heaviest measured $\delta^{56}$Fe of +0.01‰.

### 3.2. Santa Barbara Basin

Similar to the San Pedro Basin, Fe concentrations in the Santa Barbara Basin are highest near the bottom of the basin, and $\delta^{56}$Fe values are at their lowest (Table 1, Fig. 4). However, the Fe concentrations here ([Fe] = 29.5 nM) are about four times higher than in the San Pedro Basin and $\delta^{56}$Fe is lighter (−3.45‰). There is not a shallow maximum in Fe concentrations in the Santa Barbara Basin, although $\delta^{56}$Fe values do tend to get slightly lighter towards shallower depths, decreasing from $\delta^{56}$Fe = −0.29‰ at 430 m to $\delta^{56}$Fe = −1.42‰ at 30 m. In the 10 m sample closest to the surface, the iron isotope signature is heavier than in samples below, increasing to $\delta^{56}$Fe = −1.00‰.

## 4. DISCUSSION

### 4.1. San Pedro Basin

Below 700 m in the San Pedro Basin, dissolved iron concentrations increase towards the bottom while dissolved $\delta^{56}$Fe decreases. Because the San Pedro Basin has a broad flat floor and is silled below 740 m, we interpret the profile as reflecting primarily vertical transport of Fe which suggests a source of isotopically light Fe from the bottom of the basin. This is consistent with the release of dissolved Fe(II) from the sediments. The $\delta^{56}$Fe at the bottom of the San Pedro Basin is also consistent with a sedimentary Fe(II) source. Both porewater profiles and benthic flux chamber measurements point to a flux of isotopically light Fe from reducing sediments (Severmann et al., 2006, 2010). Although oxygen concentrations in the water column (typically 2–5 μM (Section 2.1.1)) are much higher than in anoxic sediment porewaters, the Fe released from these porewaters clearly persists in the water column where we observe high [Fe] and low $\delta^{56}$Fe (Fig. 3).

A second maximum in iron concentrations is observed at 50–150 m. As in the deep basin, higher Fe concentrations are correlated with lower $\delta^{56}$Fe, suggesting that this maximum is also due to the release of Fe from sediment porewa-

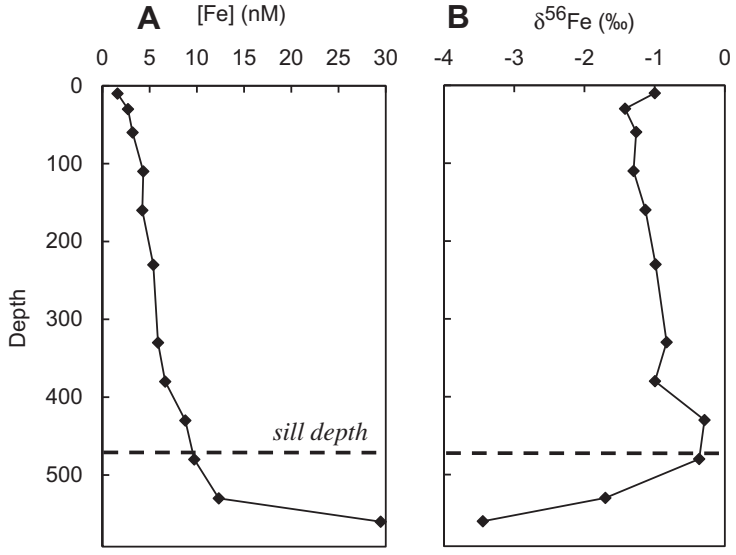


Fig. 4. Dissolved iron concentration (A) and $\delta^{56}Fe$ (B) in the Santa Barbara Basin.

ters into the water column. The topography of the San Pedro Basin supports this assumption, as the basin is surrounded by broad shallow shelves (Fig. 1). A histogram of sediment surface area by depth in the basin corresponds neatly to the observed Fe concentration maxima and $\delta^{56}Fe$ minima in both deep and shallow waters (Fig. 3).

The concentrations of Fe in surface waters (0.26 and 0.57 nM at 35 and 15 m, respectively) are lower than the waters below. The minimum in [Fe] at 35 m corresponds to the chlorophyll maximum, reflecting the biological uptake of Fe as a nutrient. Fe concentrations decrease 96% and $\delta^{56}Fe$ increases by 0.24‰ between 50 and 35 m, suggesting a biological isotope effect of $\Delta\delta^{56}Fe_{biological\text{-}seawater} = -0.09‰$, if iron isotopes were controlled by Rayleigh distillation alone. Given the large [Fe] and $\delta^{56}Fe$ gradients and rapid vertical mixing near the surface, however, an assumption of Rayleigh distillation cannot be justified and the true biological isotope effect could be either higher or lower. Above the chlorophyll maximum (at 15 m) the iron concentration increases again but, unlike the other [Fe] maxima which are associated with isotopically light Fe, the $\delta^{56}Fe$ at 15 m is the heaviest in the water column at $\delta^{56}Fe = 0‰$. This is similar to the isotopic composition of aerosol samples which generally range from about 0 to +0.2‰ (Beard et al., 2003; Waeles et al., 2007; Flament et al., 2008; Majestic et al., 2009), and to surface seawater $\delta^{56}Fe$ of +0.35‰ in the North Atlantic which is heavily impacted by dust deposition (John and Adkins, 2012), suggesting that the increase in Fe concentration at 15 m is due to the input of atmospheric dust.

### 4.2. Santa Barbara Basin

A similar pattern of high dissolved [Fe] and low $\delta^{56}Fe$ was observed in the deep Santa Barbara Basin. Again, we attribute this feature to the release of isotopically light Fe from sediment porewaters into the overlying water column. The lightest iron isotope ratios ($\delta^{56}Fe = -1.70‰$ at 530 m and $\delta^{56}Fe = -3.45‰$ at 560 m) are found in the core of the silled basin where the water column is isolated from horizontal flushing and Fe released from sediments can accumulate. The heaviest iron isotope ratios ($\delta^{56}Fe = -0.29‰$ at 430 m and $\delta^{56}Fe = -0.38‰$ at 480 m) are found close to the sill depth of 475 m. These iron isotope ratios are more similar to continental $\delta^{56}Fe$. Perhaps this feature results from a high concentration of resuspended sedimentary colloids from the nephloid layer at the basin sill, or from oxic leaching of Fe from nephloid-layer particulates as seen near Papua New Guinea (Radic et al., 2011). Alternatively, this feature could reflect a water mass that has lost a high proportion of it's dissolved phase iron to precipitation, with a negative isotope effect for precipitation (see below). As was observed in the San Pedro Basin, there is an increase in dissolved $\delta^{56}Fe$ from 35 m towards the surface at 10 m which we hypothesize results from the atmospheric deposition of Fe into the surface ocean.

### 4.3. Physical and chemical modeling of the iron isotope cycle

The qualitative picture of iron isotope cycling presented above describes the important processes that control the distribution of iron concentrations and iron isotope ratios in the San Pedro and Santa Barbara Basins. However, in order to extrapolate from these California borderland basins to understand the importance of reducing continental margin sediments in the global iron cycle, it is important to generate quantitative predictions about the sources and sinks for iron. Rayleigh distillation and two end-member mixing are the simplest ways to describe relationships between [Fe] and $\delta^{56}Fe$ (Fig. 5). However, two end-member mixing does a poor job of reproducing the observed relationship between [Fe] and $\delta^{56}Fe$ in the San Pedro Basin. Rayleigh distillation provides a reasonable fit to the data in the deepest San Pedro Basin given an isotope effect of −0.7‰ ($\alpha = 1.0007$), but poorly reproduces the observed data in the upper portion of the basin. Also, a Rayleigh

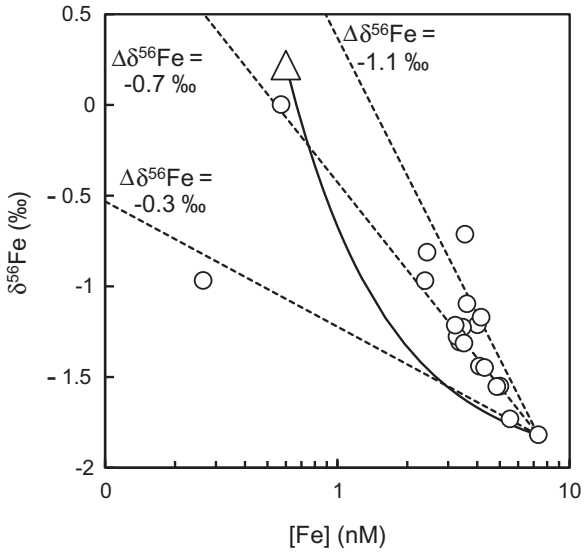


Fig. 5. The relationship between dissolved Fe concentration and $\delta^{56}$Fe in the San Pedro Basin (circles). Dashed lines represent the theoretical Rayleigh distillation of Fe isotopes during Fe precipitation from deepest San Pedro Basin waters with various isotope effects. The solid line represents a theoretical mixing between these waters and open-ocean Pacific seawater (triangle, as represented by a sample from 849 m at 0°N 180°E (Radic et al., 2011)).

distillation model does not account for the vertical mixing which we know occurs in the San Pedro Basin.

Interpreting our data in a physical–chemical model allows us better reflect the processes which we know to be important. In the San Pedro Basin, previous datasets provide estimates of physical parameters such as the upwelling rate and vertical turbulent diffusivity (mixing) in the basin. Through modeling, we can estimate (i) the magnitude of the sedimentary Fe flux, (ii) the timescale at which Fe is lost from the dissolved phase, (iii) the iron isotope composition of Fe coming out of the sediments, and (iv) the isotope effect of precipitation.

#### 4.3.1. Model design

Because the San Pedro is a silled basin below 740 m, we can neglect horizontal flow of water into or out of the basin, and we model iron cycling as a simple one-dimensional vertical process below this depth (Fig. 6). Water exchange is parameterized with estimates of vertical upwelling ($\omega$) and turbulent diffusivity ($\kappa$). Additionally, we consider the input of iron to the basin from the sediments, and the loss of dissolved iron by a first order process. Fe may be lost from the dissolved phase by adsorption of Fe ions onto Fe oxyhydroxides particles formed in the water column, resuspended sediments, or falling particulate material from higher in the water column (including biological particles), or by adsorption of Fe ions onto colloids which are subsequently adsorbed onto particles (i.e. colloidal pumping). For the sake of simplicity, and because we do not have the information to parse these different pathways, we consider all of these processes together as 'precipitation' and parameterize them using a single rate constant and a single isotope effect. At steady state, the equation for the concentration of iron at any level in the basin can therefore be given as:

$$\frac{\partial C}{\partial t} = 0 = \kappa \frac{\partial^2 [\mathrm{Fe}]}{\partial z^2} - \omega \frac{\partial [\mathrm{Fe}]}{\partial z} - k_{\mathrm{ppt}} [\mathrm{Fe}] + F_z \quad (1)$$

where $z$ is the vertical depth, [Fe] is the iron concentration at depth $z$, $k_{\mathrm{ppt}}$ is the precipitation rate constant for dissolved Fe, and $F_z$ is the flux of Fe from the sediments at depth $z$. For the top boundary condition we set the iron concentration equal to the measured [Fe] from near the top of the basin (4.08 nM at 750 m). We specify that upwelling is driven by the input of water to the bottom of the basin with this same iron concentration to reflect a source of cold water entering the basin from over the sill.

Values for vertical turbulent diffusivity ($\kappa$) and upwelling ($\omega$) are based on estimates from previous studies, combined with temperature data collected at the time of sampling. Four separate studies of $\kappa$ in the San Pedro Basin prescribe a range from 1 to 3 $\mathrm{cm^2\ s^{-1}}$ (Section 2.1.1). The relationship between $\kappa$ and $\omega$ is calculated based on the scale height $z^*$ according to the technique of Munk

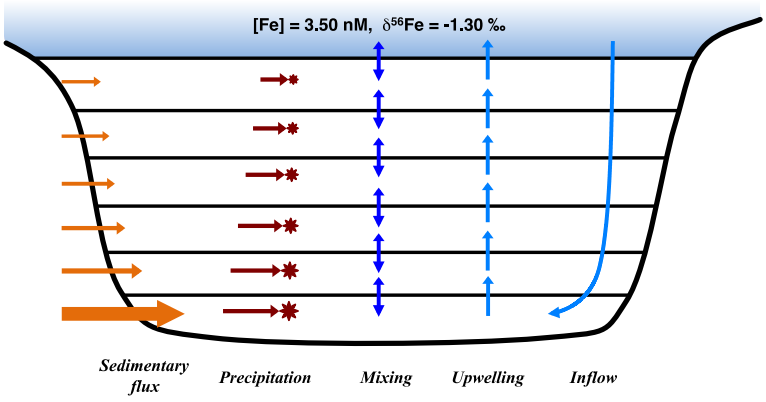


Fig. 6. Our model of the iron cycle in the San Pedro Basin considers four basic processes: sedimentary Fe flux, precipitation (all processes by which Fe is lost from the dissolved phase including adsorption to both Fe oxyhydroxide and other particles), vertical mixing, and upwelling. The [Fe] and $\delta^{56}$Fe of inflowing water are specified by the boundary conditions in the top box (shaded area).

(1966), where $z^* = \kappa/\omega$. Calculations of $z^*$ are only valid for one-dimensional diffusion and upwelling between two end members. The validity of this assumption is confirmed because temperature and salinity have a linear relationship in the deep San Pedro Basin (Fig. 7). The best fit to the observed temperature profile between 740 and 860 m from the October 2008 SPOT cruise is for $z^* = 47$ m. Vertical eddy diffusivities of 1–3 $cm^2\ s^{-1}$ (Section 2.1.1) therefore correspond to upwelling rates of 67–201 m $y^{-1}$. These upwelling rates are slightly greater than the 20–50 m $y^{-1}$ range predicted by Hammond et al. (1990) from the distribution of $^{228}Ra$. However, temperature data from the period of $^{228}Ra$ sampling correspond to $z^* = 143$ m, suggesting that upwelling rates in the basin may in fact have been slightly lower at that time compared to the time of our sampling.

The flux of Fe from the sediments at depth $z$ in the water column ($F_z$) is calculated by:

$$F_z = F_{sed}\frac{s_z}{v_z} \tag{2}$$

where $F_{sed}$ (μmol $m^{-2}\ d^{-1}$) is the flux of iron from one square meter of sediment, and $s_z/v_z$ is the ratio of sediment surface area to the total water volume of the layer into which the sedimentary flux is being diluted at depth $z$, derived from maps of basin topography.

Using Eq. (1), the iron concentration at any level in the basin can then be solved for specified values of $k_{ppt}$ and $F_{sed}$. Because we do not have any *a priori* knowledge of these quantities, we test a range of values for these variables and searching for values which produce the best match between the modeled and observed iron concentration profiles. Model profiles are generated by solving the discrete form of Eq. (1) at 151 depths between 750 and 900 m in Matlab using matrix inversion techniques.

The iron stable isotope ratio ($\delta^{56}Fe$) is calculated by constructing a similar model of iron cycling for the minor isotope $^{54}Fe$. We set the $\delta^{56}Fe$ of the water column above 750 m and of the water flowing into the deepest box to $\delta^{56}Fe = -1.44‰$, which is equal to our measured $\delta^{56}Fe$ at 750 m. The $^{54}Fe$ precipitation rate constant ($k'_{ppt}$) and flux of $^{54}Fe$ from the sediments ($F'_{sed}$) are specified in order to solve for the Fe isotope profile, and different values $k'_{ppt}$ and $F'_{sed}$ are tested in order to find a good match between modeled and observed $\delta^{56}Fe$. In typical isotopic notation, we can express the stable isotope ratio of the Fe flux from the sediments as:

$$\delta^{56}Fe_{sed} = \left(\frac{F'_{sed}/F_{sed}}{[^{54}Fe]_{IRMM\text{-}014}/[Fe]_{IRMM\text{-}014}} - 1\right)\cdot 1000 \tag{3}$$

and we can express the isotope effect for Fe precipitation in the water column as:

$$\Delta\delta^{56}Fe_{ppt} = (k_{ppt}/k'_{ppt} - 1)\cdot 1000 \tag{4}$$

### 4.3.2. Modeling results

*4.3.2.1. [Fe] profiles.* Using this simple model of iron cycling in the water column, we examine the magnitudes of four different processes which control iron concentration profiles: mixing, upwelling, sedimentary input, and precipitation. These processes correspond to the four terms in Eq. (1). At steady state, each of these terms can be either positive or negative, but they must sum to zero. The relative importance of these processes can be seen in their contribution to the iron concentration budget at each depth (Fig. 8). Precipitation results in a loss of iron from the water column, with loss rates being slightly higher towards the bottom of the basin where Fe concentrations are higher. The sedimentary flux of iron into the water column strongly increases Fe concentrations at the base of the water column, and has a much smaller contribution away from the basin bottom where the surface area of sediments is smaller. Upwelling has a relatively small positive contribution to the iron budget by bringing higher-[Fe] waters up from be-

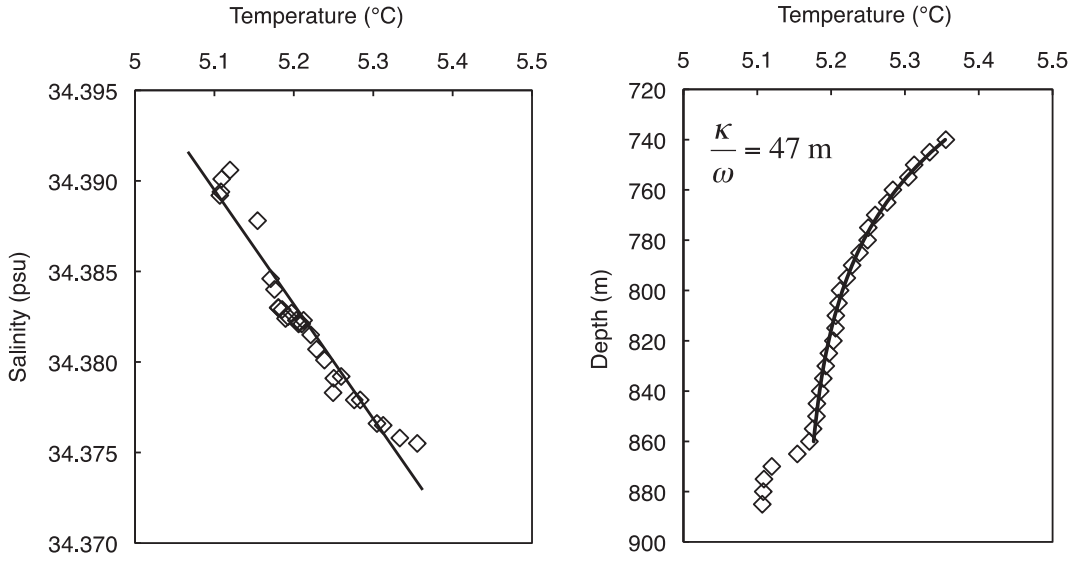


Fig. 7. There is a linear relationship between T and S in the deep San Pedro Basin below 740 m, indicating that hydrography is set by mixing between deep and shallow end-member water types. The curvature in the $T$ profile with depth is used to calculate a the ratio of vertical mixing and upwelling as $\kappa/\omega = 47$ m.

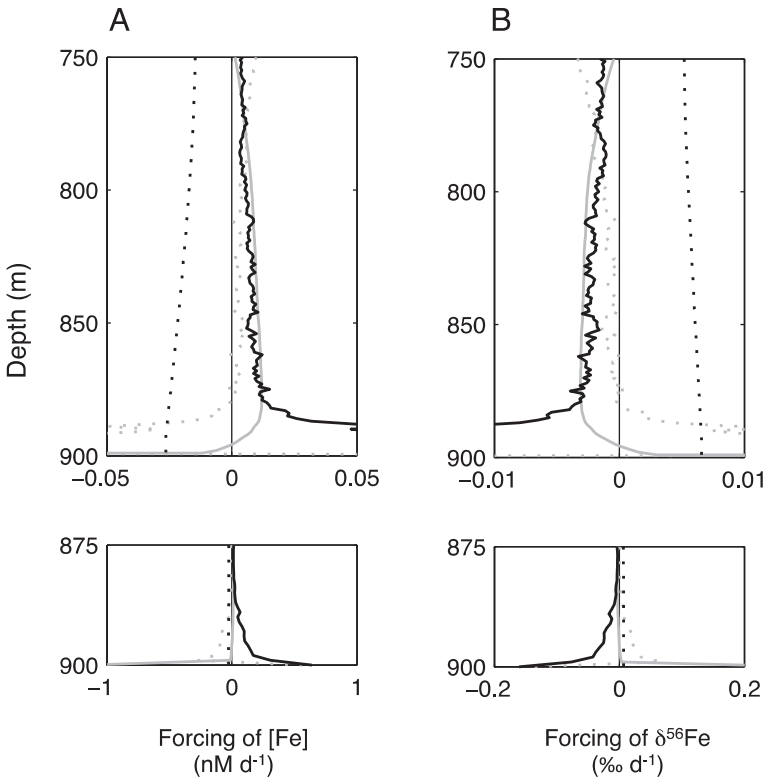


Fig. 8. The magnitude of four different processes which set the iron concentration at each depth in our model (A). Shown is the change in iron concentration (nM $d^{-1}$) resulting from upwelling (solid gray line), mixing (dashed gray line), sedimentary influx of dissolved Fe (solid black line), and precipitation (black line). Because our model solves for the [Fe] at steady state, the sum of all processes is equal to zero. In the deepest waters, a large sedimentary flux of Fe is balanced mostly by rapid mixing away of Fe. In the upper water column, the concentration of Fe is controlled most strongly by the rate of precipitation. The same four processes force the $\delta^{56}$Fe profile (B). Because the effect of a process on the dissolved $\delta^{56}$Fe is a function of both the $\delta^{56}$Fe of the iron being gained or lost from each box, and the total amount of iron gained or lost, the patterns seen here are similar to those for Fe concentrations. Data shown here are for a turbulent diffusivity of $\kappa = 2\ cm^2\ s^{-1}$ and the magnitude of forcing will change in proportion to $\kappa$, though the relative importance of the different processes remains the same.

low, except at the bottom of the basin where the input of lower-[Fe] water is a dramatic negative contribution to the iron concentration budget. Mixing, which responds strongly to non-linearity in iron concentration gradients, has a strong negative contribution to the [Fe] budget at the bottom of the basin where the [Fe] profile is concave, and a less strong positive impact higher in the water column where the [Fe] profile is convex upwards.

The two parameters which largely determine the shape of the concentration profile are sedimentary Fe flux ($F_{sed}$) and the precipitation rate constant ($k_{ppt}$). By comparison, upwelling has a relatively minor impact on the iron budget and mixing responds to the concentration gradients produced by the other processes. In general, there is a tradeoff between $F_{sed}$ and $k_{ppt}$ because sedimentary iron flux is a source of Fe to the water column and precipitation is a sink for Fe. Thus, when one of the parameters is increased, the best fit is obtained by increasing the other parameter as well (Fig. 9). However, we find that these two processes act most strongly in different parts of the water column and therefore there is a unique combination of $F_{sed}$ and $k_{ppt}$ for which the best fit is obtained. Above ~880 m, precipitation is the largest single term in the steady-state iron budget. Below ~880 m, the budget is dominated by sedimentary Fe flux and the mixing necessary to balance this Fe input. Given our *a priori* knowledge of $\kappa$ and $\omega$, the value of $F_{sed}$ is therefore most important in determining model [Fe] at the base of the water column, while $k_{ppt}$ affects the curvature of the profile and determines the goodness of fit at the top of the water column. Because of this trade-off there is a single combination of values for $F_{sed}$ and $k_{ppt}$ which produce a best fit to the data. Changing either of these terms decreases the goodness of fit even if the other term is adjusted to compensate. As vertical mixing ($\kappa$ increases, the best-fit values of $F_{sed}$ and $k_{ppt}$ increase proportionally (Fig. 10). Essentially, $\kappa$ sets the rate of vertical mixing and upwelling (which is related to $\kappa$ by the scaling height $\kappa/\omega$) and the rates of $F_{sed}$ and $k_{ppt}$ both change proportionally to maintain the same magnitude and curvature in the model [Fe] profile.

By selecting for the best fit to between the model and data, we predict a sedimentary iron flux ($F_{sed}$) between 0.32 and 0.95 $\mu mol\ m^{-2}\ d^{-1}$, and a precipitation rate constant ($k_{ppt}$) of $1.8{\cdot}10^{-3}$ to $5.3{\cdot}10^{-3}\ d^{-1}$, for values of $\kappa$ between 1 and 3 $cm^2\ s^{-1}$, respectively (Fig. 10). Perhaps the biggest uncertainty in our estimates is the assumption of a steady-state Fe distribution. In fact, the temperature profile in the deep basin shows evidence of a recent pulse of colder

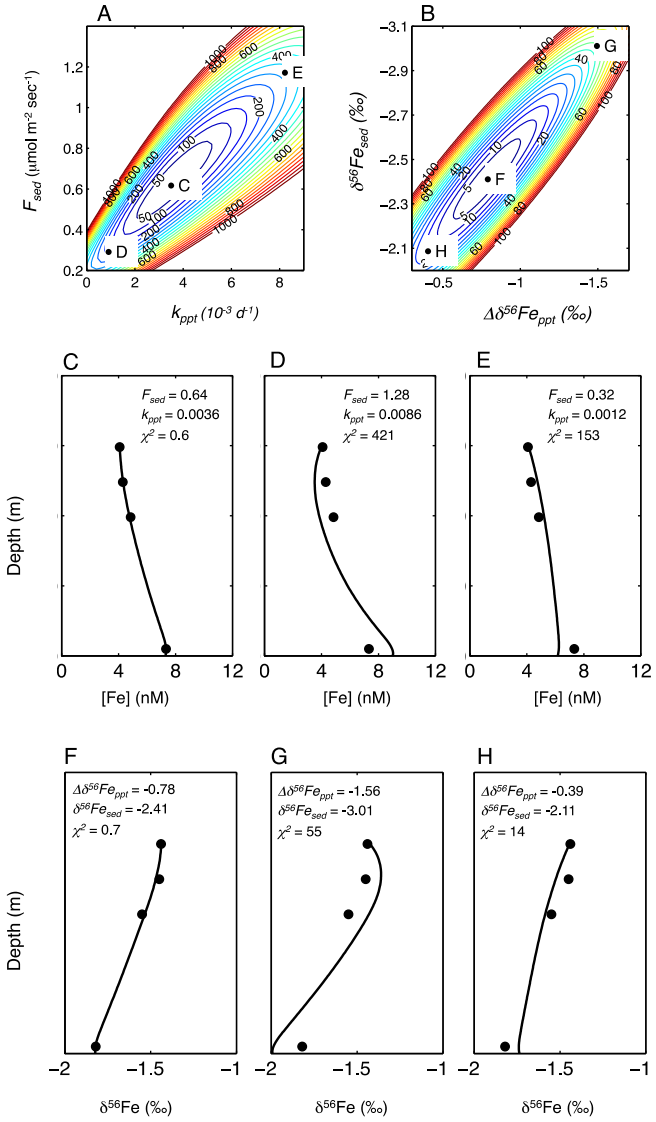


Fig. 9. Goodness of fit between data and model predictions is evaluated using a reduced $\chi$-squared, given the physical constraints of mixing and upwelling in the basin (shown here $\kappa = 2$ cm$^2$ s$^{-1}$). The match between modeled and observed Fe concentrations is optimized at a single value of $F_{sed}$ and $k_{ppt}$ (panel A, point C), though the larger errors caused by an increase or decrease in sedimentary Fe flux can be somewhat offset by a proportional change in the precipitation rate (A). Similarly, reduced $\chi$-squared error is minimized at a single value of $\delta^{56}Fe_{sed}$ and $\Delta\delta^{56}Fe_{ppt}$ (panel B, point F), with changes in $\Delta\delta^{56}Fe_{ppt}$ requiring proportional changes in $\delta^{56}Fe_{sed}$ in order to minimize error (B). In order to better illustrate the sources of error, we show both the best fit between model and observed [Fe] (C) and profiles forced with higher (D) and lower (E) values of $F_{sed}$. Below, we show both the best fit between model and observed $\delta^{56}$Fe (F) and profiles forced with lower (G) and higher (H) values of $\Delta\delta^{56}Fe_{ppt}$.

water into the bottom of the basin, with a temperature offset of about 0.7 °C between waters above 860 m and those below (Fig. 7). If we assume that this pulse of water had the temperature characteristics of the coldest waters measured during flushing of the San Pedro Basin (4.85 °C, (Berelson, 1991)), this implies a ~20% contribution of inflowing water below 860 m from the recent pulse. Because our estimate of $F_{sed}$ is highly dependent on the [Fe] measured at 895 m, our model may underestimate the true Fe flux by up to 20%, and so we extend the estimated range of sedimentary Fe fluxes to 0.32–1.14 μmol m$^{-2}$ d$^{-1}$. Because values of $k_{ppt}$ are set largely by curvature in the [Fe] profile higher in the water column, we do not make any adjustment to the range predicted by our model.

The precipitation rate constants predicted by our model ($k_{ppt} = 1.8{\cdot}10^{-3}$ to $5.3{\cdot}10^{-3}$ d$^{-1}$) are equivalent to dissolved Fe half-lives of 131–394 days, or precipitation timescales of approximately 0.5–1.5 years (Fig. 10). In order to apply these constants to the open ocean, they must reflect the precipitation of Fe(III), which is the dominant form of Fe in oxic seawater. While Fe is released from the sediments as Fe(II), our calculations of the timescale for Fe precipitation are much longer than the time constant for Fe(II) oxidation. Typical $O_2$ concentrations in the deep San Pedro basin

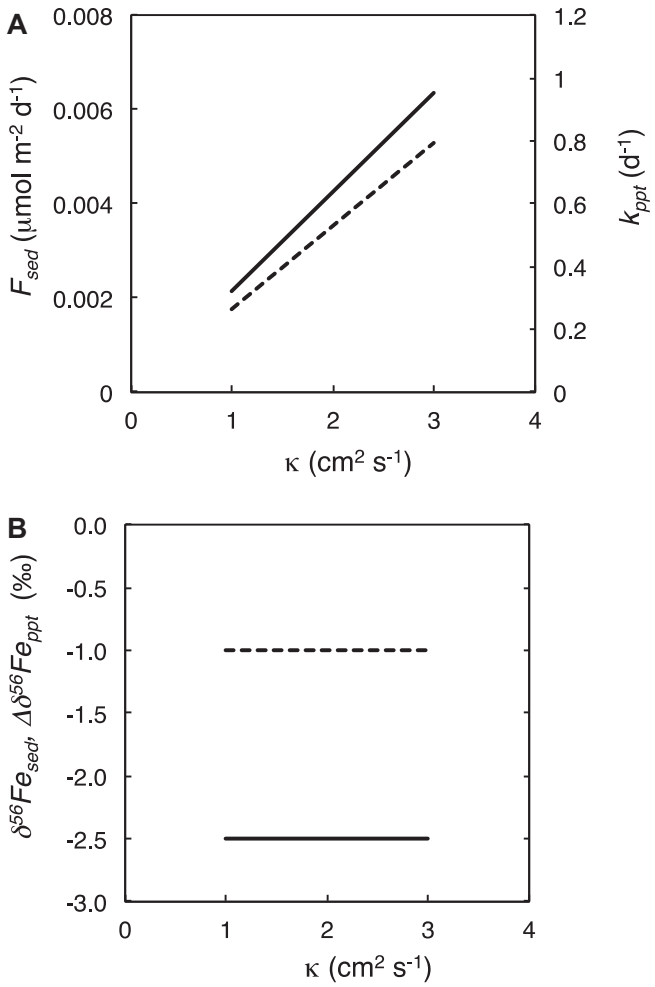


Fig. 10. As the turbulent diffusivity ($\kappa$) is increased, our model predicts a proportional increase in both the sedimentary Fe flux ($F_{sed}$, solid line) and the rate constant for precipitation ($k_{ppt}$, dashed line) in order to fit the observed Fe concentration data (A). Varying $\kappa$ has no impact on the model predicted values of the Fe isotope ratio of the flux ($\delta^{56}Fe_{sed}$, solid line) or the isotope effect for precipitation ($\Delta\delta^{56}Fe_{sed}$, dashed line) (B).

are about 5 µmol kg$^{-1}$ (Berelson, 1991), and typical pH values are ~7.6 (Berelson, 1985). Based on the data of Millero et al. (1987), we predict an Fe(II) oxidation timescale of 5.5 days at a temperature of 5 °C. Over this timescale, vertical mixing only transports a few percent of bottom water more than 5 m above the bottom, and upwelling is only 1–3 m. We therefore expect that most Fe(II) oxidizes within a few meters of the bottom. Because Fe is largely oxidized within a few meters of the sediments, while the strongest constraint on $k_{ppt}$ is the shape of the [Fe] profile throughout the entire 160 m silled basin, we take the model predicted $k_{ppt}$ as the rate constant for loss of dissolved Fe(III) from the water column. Thus, $k_{ppt}$ reflects the rate at which dissolved or colloidal Fe(III) is converted to particulate Fe(III), rather than the conversion of Fe(II) to Fe(III).

*4.3.2.2. $\delta^{56}$Fe profiles.* Using a similar approach as above, we explore the parameters which are most importance in setting the dissolved $\delta^{56}$Fe profile in our model. Mixing, upwelling, and sedimentary Fe flux all contribute to a decrease in $\delta^{56}$Fe which is balanced by an isotope effect of precipitation which leaves the dissolved phase isotopically heavier (Fig. 8). Similar to the case with the Fe concentration profiles, we find that one parameter ($\delta^{56}Fe_{sed}$) has a large influence on the match between modeled and observed $\delta^{56}$Fe in the deepest water sample, while another parameter ($\Delta\delta^{56}Fe_{ppt}$) is most strongly responsible for setting the curvature of modeled $\delta^{56}$Fe with depth (Fig. 9). However in contrast to the modeled Fe concentrations, different values of $\kappa$ do not affect $\delta^{56}Fe_{sed}$ and $\Delta\delta^{56}Fe_{ppt}$ values at which the best fit between model and observed $\delta^{56}$Fe is found. The best fit is obtained with $\delta^{56}Fe_{sed} = -2.42‰$ and $\Delta\delta^{56}Fe_{ppt} = -0.80‰$, regardless of changes in $\kappa$ and $\omega$ Fig. 1.

The model-predicted iron isotope ratio of the sedimentary iron flux ($\delta^{56}Fe_{sed} = -2.4‰$, as expressed at 5 m above the bottom) is similar to porewater and benthic flux chamber $\delta^{56}$Fe measurements, despite large variations in the estimated magnitude of flux (Fig. 11). Benthic flux chamber $\delta^{56}$Fe values range between −0.7‰ and −4.0‰ at several locations on the continental shelf off the coast of California and Oregon, and porewater $\delta^{56}$Fe at the sediment–water

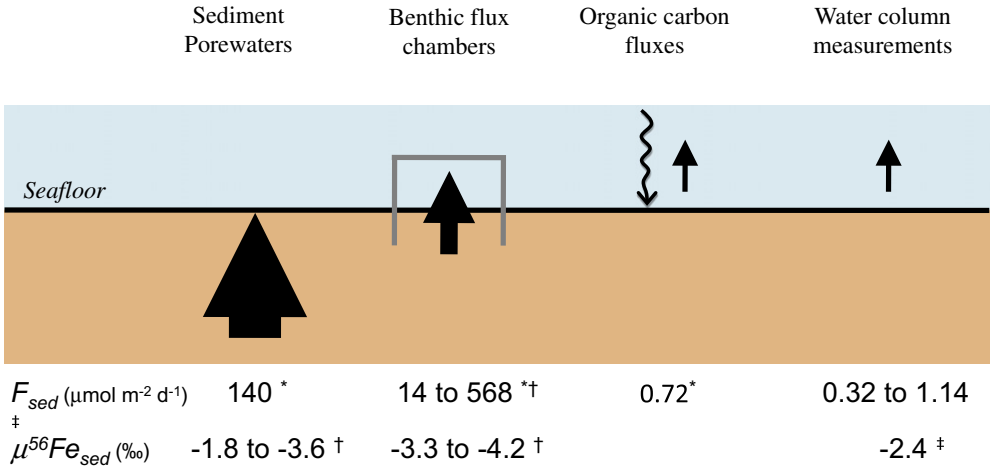


Fig. 11. The rate of Fe flux from sediments in the San Pedro Basin ($F_{sed}$) and isotopic composition of that flux ($\delta^{56}Fe_{sed}$) as predicted by different methods. Fe fluxes have been predicted from sediment porewater [Fe] profiles (Elrod et al., 2004), by monitoring [Fe] in benthic flux chambers (Elrod et al., 2004; Severmann et al., 2010), from a regional relationship between organic carbon flux to the sediments and benthic flux chamber measurements, and from water column measurements (Elrod et al., 2004). Porewater $\delta^{56}Fe$ measurements are not available for the San Pedro Basin, so we apply the range of core-top porewater $\delta^{56}Fe$ measurements from other California Borderland basins, while benthic flux chamber and water column $\delta^{56}Fe_{sed}$ estimates are based on San Pedro Basin measurements (Severmann et al., 2010, this work). While the estimated variations in Fe flux span four orders of magnitude, the isotopic composition of this flux remains relatively constant between −2.4‰ and −4.2‰.

interface is between −1.8‰ and −3.6‰ (Severmann et al., 2006, 2010). In the San Pedro Basin specifically, benthic flux chamber $\delta^{56}Fe$ values ranged from −3.29‰ to −4.16‰ over a 34 h period (Severmann et al., 2010). If the variations in Fe flux predicted from sediment porewater profiles, benthic flux chambers, and water column measurements represent actual differences in Fe flux in the sediments, at the sediment water interface, and into the water column, it is perhaps surprising that $\delta^{56}Fe$ varies so little. With so much Fe precipitation at the sediment water interface, even a small isotope effect during precipitation could have a large impact on $\delta^{56}Fe$ due to Rayleigh distillation. The relatively invariable $\delta^{56}Fe$ values may therefore be best explained by isotopic reequilibration between Fe(II) and Fe(III) in both the sediments and somewhere in the bottom few meters of the water column. The rate of redox isotopic equilibration depends on both ambient temperature and total iron concentrations (Welch et al., 2003). For example, in 5 °C bottom waters with Fe(II) and exchangeable-Fe(III) concentrations of 7 nM each, we predict an isotopic equilibration timescale of about 100 h. However, in sediment porewaters or the nephloid layer, where particulate and dissolved iron concentrations are orders of magnitude higher, the timescale for Fe(II)–Fe(III) isotopic equilibration will be correspondingly orders of magnitude shorter. The invariance in dissolved $\delta^{56}Fe$ as measured by different techniques in the San Pedro and other California borderland basins suggests that a single process (rapid Fe(II)–Fe(III) isotopic equilibration) will set a characteristically light $\delta^{56}Fe$ value for the flux from all reducing continental margin sediments.

Our model predicts an isotope effect of $\Delta\delta^{56}Fe_{ppt} = -0.8‰$ for first-order loss of dissolved Fe from the water column. Because we predict that Fe is mostly oxidized within a few meters of the bottom (Section 4.3.2.1), this isotopic fractionation is unlikely to reflect redox processes. However, a kinetic isotope effect would result in the preferential precipitation of lighter Fe isotopes, and our model-predicted $\Delta\delta^{56}Fe_{ppt}$ is similar to the −1.3‰ kinetic isotope effect for precipitation of hematite from aqueous Fe(III) in 0.05 N $HNO_3$ (Skulan et al., 2002). Thus, we hypothesize that $\Delta\delta^{56}Fe_{ppt}$ reflects a kinetic isotope effect during the transfer of Fe(III) ions from the dissolved phase onto particulates.

### 4.4. Santa Barbara Basin iron isotope cycling

The sampling distribution in the Santa Barbara Basin does not allow us to model the Fe isotope cycle here as we have done for the San Pedro Basin. There are only three samples taken below the sill depth, and the deepest sample at 560 m is 30 m above the basin floor. Without an accurate measurement of [Fe] and $\delta^{56}Fe$ close to the basin floor, there is little constraint on the magnitude of the sedimentary Fe flux ($F_{sed}$) or on the $\delta^{56}Fe$ of this flux ($\delta^{56}Fe_{sed}$). Without a constraint on these values, there is not enough data to constrain the precipitation rate constant ($k_{ppt}$) or isotope effect of precipitation ($\Delta\delta^{56}Fe_{ppt}$).

However, the Santa Barbara Basin iron isotope profile is qualitatively similar to the San Pedro Basin. Iron concentrations are highest and $\delta^{56}Fe$ values are lowest near the bottom of the basin. This is consistent with the release of isotopically light Fe from sediments and a preferential loss of isotopically light Fe during precipitation. The $\delta^{56}Fe$ at 560 m in the Santa Barbara Basin (−3.45‰) is lighter than the lightest measured value from the San Pedro Basin (−1.82‰) or even than the model predicted $\delta^{56}Fe$ of the sedimentary flux (−2.5‰). However this value is similar to the predicted Fe(II)–Fe(III) equilibrium isotope effect of −3.40‰ at 6.5 °C (Welch et al., 2003) and similar to the average benthic flux chamber $\delta^{56}Fe$ in the San Pedro

and Santa Barbara Basins of −3.54‰ (Severmann et al., 2010), again suggesting a characteristically light $\delta^{56}$Fe signature from all reducing continental margin sediments.

### 4.5. The global flux of Fe and Fe isotopes from reducing continental margins

#### 4.5.1. Fe concentration fluxes

Previous estimates of sedimentary dissolved Fe flux in the San Pedro Basin vary by about four orders of magnitude, with our estimates falling at the lower end of this range (Fig. 11). Severmann et al. (2010) report an iron flux of 568 ± 215 μmol $m^{-2}$ $d^{-1}$ based on benthic flux chamber data. Elrod et al. (2004) report an estimate of 14.4 μmol $m^{-2}$ $d^{-1}$ using benthic flux chamber [Fe] measurements, and a flux of 140 μmol $m^{-2}$ $d^{-1}$ using porewater dissolved [Fe] profiles. Elrod et al. also have derived a relationship between the flux of organic carbon to sediments and the flux of dissolved Fe back out of the sediments by using benthic flux chamber data from several locations along the coast of the western United States. This relationship predicts a sedimentary Fe flux of 0.72 μmol $m^{-2}$ $d^{-1}$ in the San Pedro basin, which is within our model-predicted range of 0.32–1.14 μmol $m^{-2}$ $d^{-1}$. We propose that the range in various estimates reflects an actual decrease in dissolved Fe fluxes with vertical height, as opposed to seasonal variability or flawed methodology, with rapid Fe precipitation occurring at the sediment–water interface and in the bottom few meters of the water column. Organic carbon fluxes measured in San Pedro Basin sediment traps varied by only a factor of ~3 over a seven month period (Thunell et al., 1994), and assuming a linear relationship between organic carbon and dissolved Fe flux (Elrod et al., 2004), variations in organic carbon flux could only account for a small fraction of the total difference between various estimates of sedimentary dissolved Fe flux. Instead, we propose that the 140 μmol $m^{-2}$ $d^{-1}$ Fe fluxes measured by Elrod et al. (2004) using porewater iron concentration profiles may actually represent the upwards flux of dissolved Fe within the sediments, while the 14.4 μmol $m^{-2}$ $d^{-1}$ flux they measured in benthic flux chambers measures the amount of Fe that escapes across the sediment–water interface into the bottom few cm of the water column. The difference between these two estimates would therefore imply precipitation of Fe at (or very close to) the sediment–water interface. The estimate of 568 ± 215 μmol $m^{-2}$ $d^{-1}$ dissolved iron flux based on benthic flux chamber data (Severmann et al., 2010) does not match our overall conceptual model of Fe fluxes decreasing from the sediments to the water column, but it could be explained if decreasing oxygen concentrations in the benthic flux chamber caused the zone of precipitation to move above the sediment–water interface. Our estimate of a 0.32–1.14 μmol $m^{-2}$ $d^{-1}$ dissolved Fe flux at 5 m above the bottom may also be accurate, despite being orders of magnitude lower than estimates based on porewater and benthic flux chamber data, if the difference between various estimates are accounted for by Fe precipitation in the bottom few meters of the water column. This depth range matches the spatial scale over which we predict sedimentary Fe(II) will oxidize in the San Pedro Basin. We therefore hypothesize a relatively fast process of Fe removal that dominates in the bottom few meters of the water column where Fe(II) is oxidized to Fe(III), while higher in the water column precipitation is dominated by the slower process of Fe(III) precipitation represented in our model by $k_{ppt}$.

The fact that Fe is already oxidized by 5 m above the bottom in the San Pedro Basin might help to explain the similarity between our estimates of dissolved Fe flux and those based on the regional relationship between organic carbon deposition and dissolved Fe fluxes in benthic flux chambers (0.32–1.14 μmol $m^{-2}$ $d^{-1}$ and 0.72 μmol $m^{-2}$ $d^{-1}$, respectively) (Elrod et al., 2004). Because the $C_{org}$:$Fe_{dissolved}$ flux relationship was developed using benthic flux chamber data from sites where bottom-water oxygen concentrations are higher than in the San Pedro Basin, we hypothesize that both our model predictions and the global $C_{org}$:$Fe_{dissolved}$ relationship developed by Elrod et al. provide an accurate representation of sedimentary dissolved Fe flux which is stabilized in the water column as Fe(III). Thus, our model uses water-column data to confirm the benthic flux chamber-based prediction of Elrod et al., lending support to the use of $C_{org}$:$Fe_{dissolved}$ in models of the global iron cycle (e.g. Moore and Braucher, 2008).

#### 4.5.2. Fe isotope fluxes

Applying the model parameters determined in the deep San Pedro basin, we can make quantitative predictions about the global flux of Fe isotopes from continental margin sediments to the open ocean (Table 2). We take our estimate of the global flux of Fe ($8.9{\cdot}10^{10}$ mol $y^{-1}$) from continental margin sediments from Elrod et al. (2004) We predict that this iron persists in the water column with a mean life of $1/k_{ppt}$, or 0.52–1.56 years. With a global Fe reservoir of $10^{12}$ mol of Fe ($1.4{\cdot}10^{21}$ $kg^3$ of seawater, $[Fe]_{avg} = 0.8$ nM), we calculate that 4–12% of the global dissolved Fe in the oceans may originate in continental margin sediments. With a flux isotope ratio ($\delta^{56}Fe_{sed}$) of −2.4‰ and an isotope effect for precipitation ($\Delta\delta^{56}Fe_{ppt}$) of −0.8‰, the average isotopic composition of sedimentary-derived Fe in the open ocean will be −1.6‰. Assuming that the bulk ocean $\delta^{56}$Fe is about +0.3‰ (Lacan et al., 2008; Radic et al., 2011; John and Adkins, 2012), the sedimentary flux lowers the total global $\delta^{56}$Fe by −0.08‰ to −0.26‰. Indeed, the lowest $\delta^{56}$Fe observed in the Southern Ocean is coincident with the minimum oxygen concentration, suggesting a possible source of this Fe from reducing continental margin sediments (Lacan et al., 2008).

## 5. CONCLUSIONS

Seawater dissolved and particulate iron in the San Pedro and Santa Barbara basins show large (several permil) variations in iron isotopes. The dominant process affecting both [Fe] and $\delta^{56}$Fe is the release of isotopically light Fe from sediments at the bottom of the basins, resulting in both the highest Fe concentrations and lowest Fe isotope ratios in the deepest samples from both the Santa Barbara and San Pedro Basin. In the San Pedro Basin, the isotopic evidence points to a secondary peak in sedimentary Fe at 50–150 m, and an atmospheric source of Fe in surface waters.

Table 2
The potential impact of continental margin Fe on the global marine iron pool. Iron precipitation timescales are calculated in this work. The continental margin flux of Fe to the ocean is taken from Elrod et al. (Elrod et al., 2004), which matches our findings in the San Pedro Basin. The amount of Fe in the global ocean assumes an average Fe concentration of 0.8 nM. Using these values, we predict that 4–12% of Fe in the global ocean derives from continental margin sediments, and that the average marine $\delta^{56}$Fe is made 0.08–0.26‰ lighter than it would be in the absence of this continental margin flux.

| | | |
|---|---|---|
| Iron precipitation timescale (y) | 0.52 | 1.56 |
| Global iron flux to the ocean (mol $y^{-1}$) | $8.9 \cdot 10^{10}$ | $8.9 \cdot 10^{10}$ |
| Total iron in the ocean (mol) | $10^{12}$ | $10^{12}$ |
| Global iron from continental margins | 4% | 12% |
| $\Delta^{56}$Fe | −0.08‰ | −0.26‰ |

In the San Pedro Basin, high resolution measurements of [Fe] and $\delta^{56}$Fe in the deep silled basin have allowed us to make quantitative predictions of four quantities which are of great importance for understanding the role of continental margins in the global iron cycle: (1) the rate at which Fe is released from sediments, (2) the time constant for Fe precipitation in the water column, (3) the isotope composition of Fe released from the sediments, and (4) the isotope effect for precipitation of Fe. Our predictions of the sedimentary Fe flux match well with a previously established global relationship between organic carbon oxidation and Fe flux. While these flux estimates are much lower than previous estimates of Fe flux in the San Pedro Basin using data from benthic flux chambers and porewater [Fe] profiles, our predictions of the $\delta^{56}$Fe of the flux match well with these methods, suggesting an Fe(II)–Fe(III) equilibrium isotope effect sets the dissolved $\delta^{56}$Fe near the sediment–water interface.

By following sedimentary Fe concentrations and isotopes into the water-column, we have been able to make the first predictions about the timescale of sedimentary Fe precipitation and the isotope effect of this precipitation. We estimate that continental shelves are a major source of Fe to the world ocean contributing 4–12% of the global iron pool. While $\delta^{56}$Fe may be used to trace this flux, both source $\delta^{56}$Fe and subsequent isotopic fractionation during Fe loss from the dissolved phase must be considered. While the flux $\delta^{56}$Fe originating from the sediments may be isotopically light, the preferential loss of lighter isotopes during precipitation will make the remaining Fe isotopically heavier, thus confounding a straightforward interpretation of isotopically light Fe as being diagnostic of Fe input from reducing continental margins. As the global patterns of Fe and Fe isotope distribution in the ocean are measured by the Geotraces program, our modeling approach can provide a framework for testing these predictions against data from the field.

## APPENDIX A. SUPPLEMENTARY DATA

Supplementary data associated with this article can be found, in the online version, at http://dx.doi.org/10.1016/j.gca.2012.06.003.

## REFERENCES


Anbar A. D., Jarzecki A. A. and Spiro T. G. (2005) Theoretical investigation of iron isotope fractionation between $Fe(H_2O)(3^+)(6)$ and $Fe(H_2O)(2^+)(6)$: implications for iron stable isotope geochemistry. *Geochim. Cosmochim. Acta* **69**, 825–837.

Archer D. E. and Johnson K. (2000) A model of the iron cycle in the ocean. *Global Biogeochem. Cycles* **14**, 269–279.

Aumont O. and Bopp L. (2006) Globalizing results from ocean in situ iron fertilization studies. *Global Biogeochem. Cycles* **20**.

Beard B. L., Johnson C. M., Von Damm K. L. and Poulson R. L. (2003) Iron isotope constraints on Fe cycling and mass balance in oxygenated Earth oceans. *Geology* **31**, 629–632.

Bennett S. A., Achterberg E. P., Connelly D. P., Statharn P. J., Fones G. R. and Gernian C. R. (2008) The distribution and stabilisation of dissolved Fe in deep-sea hydrothermal plumes. *Earth Planet. Sci. Lett.* **270**, 157–167.

Berelson W. M. (1985) Studies of water column mixing and benthic exchange of nutrients, carbon and radon in the southern California borderland. Ph. D. dissertation, Geological Sciences, University of Southern California, Los Angeles, CA, pp. 219.

Berelson W. M. (1991) The flushing of two deep-sea basins, southern California borderland. *Limnol. Oceanogr.* **36**, 1150–1166.

Berelson W. M. and Hammond D. E. (1986) The calibration of a new free-vehicle benthic flux chamber for use in the deep-sea. *Deep-Sea Res.* **33**, 1439–1454.

Berelson W. M., Hammond D. E. and Fuller C. (1982) Radon-222 as a tracer for mixing in the water column and benthic exchange in the southern California borderland. *Earth Planet. Sci. Lett.* **61**, 41–54.

Bergquist B. A. and Boyle E. A. (2006) Iron isotopes in the Amazon River system: weathering and transport signatures. *Earth Planet. Sci. Lett.* **248**, 54–68.

Boyle E. A., Bergquist B. A., Kayser R. A. and Mahowald N. (2005) Iron, manganese, and lead at Hawaii Ocean Time-series station ALOHA: temporal variability and an intermediate water hydrothermal plume. *Geochim. Cosmochim. Acta* **69**, 933–952.

Bruland K. W., Rue E. L. and Smith G. J. (2001) Iron and macronutrients in California coastal upwelling regimes: implications for diatom blooms. *Limnol. Oceanogr.* **46**, 1661–1674.

Bruland K. W., Rue E. L., Smith G. J. and DiTullio G. R. (2005) Iron, macronutrients and diatom blooms in the Peru upwelling regime: brown and blue waters of Peru. *Mar. Chem.* **93**, 81–103.

Deutsch C., Gruber N., Key R. M., Sarmiento J. L. and Ganachaud A. (2001) Denitrification and $N_2$ fixation in the Pacific Ocean. *Global Biogeochem. Cycles* **15**, 483–506.

Elrod V. A., Berelson W. M., Coale K. H. and Johnson K. S. (2004) The flux of iron from continental shelf sediments: a missing source for global budgets. *Geophys. Res. Lett.* **31**.

Flament P., Mattielli N., Aimoz L., Choel M., Deboudt K., de Jong J., Rimetz-Planchon J. and Weis D. (2008) Iron isotopic fractionation in industrial emissions and urban aerosols. *Chemosphere* **73**, 1793–1798.

Fung I. Y., Meyn S. K., Tegen I., Doney S. C., John J. G. and Bishop J. K. B. (2000) Iron supply and demand in the upper ocean. *Global Biogeochem. Cycles* **14**, 281–295.

Gruber N. and Sarmiento J. L. (1997) Global patterns of marine nitrogen fixation and denitrification. *Global Biogeochem. Cycles* **11**, 235–266.

Hammond D. E., Marton R. A., Berelson W. M. and Ku T. (1990) Radium 228 distribution and mixing in San Nicholas and San

Pedro basins, southern California borderland. *J. Geophys. Res.* **95**, 3321–3335.

Homoky W. B., Severmann S., Mills R. A., Statham P. J. and Fones G. R. (2009) Pore-fluid Fe isotopes reflect the extent of benthic Fe redox recycling: evidence from continental shelf and deep-sea sediments. *Geology* **37**, 751–754.

Jackson G. A. (1982) Sludge disposal in the Southern California Basins. *Environ. Sci. Technol.* **16**, 746–757.

John S. G. and Adkins J. F. (2010) Analysis of dissolved iron isotopes in seawater. *Mar. Chem.* **119**, 65–76.

John S. G. and Adkins J. F. (2012) The vertical distribution of iron stable isotopes in the North Atlantic near Bermuda. *Global Biogeochem. Cycles* **26**, GB2034, 10 PP. http://dx.doi.org/10.1029/2011GB004043.

Johnson C. M., Skulan J. L., Beard B. L., Sun H., Nealson K. H. and Braterman P. S. (2002) Isotopic fractionation between Fe(III) and Fe(II) in aqueous solutions. *Earth Planet. Sci. Lett.* **195**, 141–153.

Johnson K., Boyle E., Bruland K., Coale K., Measures C., Moffett J., Aguilar-Islas A., Barbeau K., Bergquist B., Bowie A., Buck K., Cai Y., Chase Z., Cullen J., Doi T., Elrod V., Fitzwater S., Gordon M., King A., Laan P., Baquer L., Landing W., Lohan M., Mendez J., Milne A., Obata H., Ossiander L., Plant J., Sarthou G., Sedwick P., Smith G., Sohst B., Tanner S., Berg S. V. d. and Wu J. (2007) Developing standards for dissolved iron in seawater. *EOS* **88**, 131–132.

Johnson K. S., Chavez F. P. and Friederich G. E. (1999) Continental-shelf sediment as a primary source of iron for coastal phytoplankton. *Nature* **398**, 697–700.

Lacan F., Radic A., Jeandel C., Poitrasson F., Sarthou G., Pradoux C. and Freydier R. (2008) Measurement of the isotopic composition of dissolved iron in the open ocean. *Geophys. Res. Lett.* **35**.

Lam P. J. and Bishop J. K. B. (2008) The continental margin is a key source of iron to the HNLC North Pacific Ocean. *Geophys. Res. Lett.* **35**, L07608.

Lam P. J., Bishop J. K. B., Henning C. C., Marcus M. A., Waychunas G. A. and Fung I. Y. (2006) Wintertime phytoplankton bloom in the subarctic Pacific supported by continental margin iron. *Global Biogeochem. Cycles* **20**.

Lohan M. C. and Bruland K. W. (2008) Elevated Fe(II) and dissolved Fe in hypoxic shelf waters off Oregon and Washington: an enhanced source of iron to coastal upwelling regimes. *Environ. Sci. Technol.* **42**, 6462–6468.

Majestic B. J., Anbar A. D. and Herckes P. (2009) Stable isotopes as a tool to apportion atmospheric iron. *Environ. Sci. Technol.* **43**, 4327–4333.

Millero F. J., Sotolongo S. and Izaguirre M. (1987) The oxidation kinetics of Fe(II) in seawater. *Geochim. Cosmochim. Acta* **51**, 793–801.

Moore J. K. and Braucher O. (2008) Sedimentary and mineral dust sources of dissolved iron to the world ocean. *Biogeosciences* **5**, 631–656.

Moore J. K., Doney S. C. and Lindsay K. (2004) Upper ocean ecosystem dynamics and iron cycling in a global three-dimensional model. *Global Biogeochem. Cycles* **18**.

Munk W. H. (1966) Abyssal recipes. *Deep-Sea Res.* **13**, 707–730.

Parekh P., Follows M. J. and Boyle E. (2004) Modeling the global ocean iron cycle. *Global Biogeochem. Cycles* **18**.

Radic A., Lacan F. and Murray J. W. (2011) Iron isotopes in the seawater of the equatorial Pacific Ocean: new constraints for the oceanic iron cycle. *Earth Planet. Sci. Lett.* **306**, 1–10.

Reimers C. E., Lange C. B., Tabak M. and Bernhard J. M. (1990) Seasonal spillover and varve formation in the Santa Barbara Basin, California. *Limnol. Oceanogr.* **35**, 1577–1585.

Sawlan J. J. and Murray J. W. (1983) Trace-metal remobilization in the interstitial waters of red clay and hemipelagic marine sediments. *Earth Planet. Sci. Lett.* **64**, 213–230.

Severmann S., Johnson C. M., Beard B. L. and McManus J. (2006) The effect of early diagenesis on the Fe isotope compositions of porewaters and authigenic minerals in continental margin sediments. *Geochim. Cosmochim. Acta* **70**, 2006–2022.

Severmann S., McManus J., Berelson W. M. and Hammond D. E. (2010) The continental shelf benthic iron flux and its isotope composition. *Geochim. Cosmochim. Acta* **74**, 3984–4004.

Skulan J. L., Beard B. L. and Johnson C. M. (2002) Kinetic and equilibrium Fe isotope fractionation between aqueous Fe(III) and hematite. *Geochim. Cosmochim. Acta* **66**, 2995–3015.

Thunell R. C., Moore W. S., Dymond J. and Pilskaln C. H. (1994) Elemental and isotopic fluxes in the southern California Bight – a time-series sediment trap study in the San Pedro basin. *J. Geophys. Res. Oceans* **99**, 875–889.

Toner B. M., Fakra S. C., Manganini S. J., Santelli C. M., Marcus M. A., Moffett J., Rouxel O., German C. R. and Edwards K. J. (2009) Preservation of iron(II) by carbon-rich matrices in a hydrothermal plume. *Nat. Geosci.* **2**, 197–201.

Waeles M., Baker A. R., Jickells T. and Hoogewerff J. (2007) Global dust teleconnections: aerosol iron solubility and stable isotope composition. *Environ. Chem.* **4**, 233–237.

Welch S. A., Beard B. L., Johnson C. M. and Braterman P. S. (2003) Kinetic and equilibrium Fe isotope fractionation between aqueous Fe(II) and Fe(III). *Geochim. Cosmochim. Acta* **67**, 4231–4250.

Wu J. F. and Boyle E. A. (1998) Determination of iron in seawater by high-resolution isotope dilution inductively coupled plasma mass spectrometry after Mg(OH)(2) coprecipitation. *Anal. Chim. Acta* **367**, 183–191.

*Associate editor:* Mark Rehkamper